Seismological estimates of means of isostatic support of the Sierra Nevada

W. Levandowski[1], C.H. Jones[1], H. Reeg[1], A. Frassetto[2], H. Gilbert[3], G. Zandt[4], and T.J. Owens[5]

[1]*Department of Geological Sciences, University of Colorado, Boulder, Campus Box 399 UCB, Boulder, Colorado 80309, USA*

[2]*IRIS, 1200 New York Ave. NW, Suite 400, Washington, District of Columbia 20005, USA*

[3]*Department of Earth, Atmospheric, and Planetary Sciences, Purdue University, 550 Stadium Mall Drive, West Lafayette, Indiana 47907, USA*

[4]*Department of Geosciences, The University of Arizona, 1040 E. 4th Street, Tucson, Arizona 85721, USA*

[5]*Department of Earth & Ocean Sciences, University of South Carolina, 701 Sumter Street, Columbia, South Carolina 29208, USA*

ABSTRACT

The modern topography of the Sierra Nevada (California, USA) has been attributed to rapid uplift following foundering of negatively buoyant lithosphere into the asthenosphere since ca. 10 Ma. Uplift now manifests as ~2 km mean topographic relief between the crest of the southern Sierra Nevada and the western foothills and 1–2 km between the Sierran crest and adjacent Basin and Range. In this study, we use seismic P-wave velocity structures derived from teleseismic tomography to estimate the lithospheric density structure in the region and thus infer the current sources of topographic support. We exploit the different derivatives of crustal density with temperature and wave speed to attempt to identify a single solution for crustal density and temperature that satisfies flexural isostasy and the P-wave tomography. This solution yields both temperature variations compatible with observed heat flow and Bouguer gravity anomalies concordant with observations. We find that the topographic gradient between the crest and the eastern Great Valley is due to both crustal and mantle sources. Despite a greater thickness, the foothills crust is less buoyant than that beneath the range crest, accounting for ~1 km of the topographic difference. High densities are due principally to composition. High-velocity upper mantle (~50–100 km depth) is also observed beneath the foothills but not the range crest, and this contrast explains an additional 1 km of topographic difference. Miocene or more recent removal of such upper mantle material from the Sierran crest, as inferred from xenoliths, would have triggered rapid uplift of ~1 km. Our findings are consistent with the removal of negatively buoyant material from beneath the Sierra Nevada since the Miocene.

INTRODUCTION

The crust beneath the Sierra Nevada (California, USA; Fig. 1) is thinner (Fliedner et al., 2000; Frassetto et al., 2011; Jones et al., 1994; Ruppert et al., 1998) and more felsic than the worldwide average (e.g., Holbrook et al., 1992), and substantially thinner under the high parts of the range than under the low western foothills (Fig. 2B). Despite this thin crust, the mean surface elevation within the range is ~2.5 km (Fig. 2A). Gravity measurements show the range to be in isostatic equilibrium or even somewhat overcompensated, i.e., having a greater gravity low than expected if the observed topography were compensated by an Airy root (Kennelly and Chase, 1989; Simpson et al., 1986). Such elevations in the absence of correlated variations in crustal thickness require lateral density variations within the crust and/or uppermost mantle (e.g., Jones et al., 1994).

The unusual crustal variations of the Sierra are matched by controversy over the origin of the topography. From the time of work by LeConte (1886) to more recent times, geologists inferred that the Sierra Nevada rose during the late Tertiary (e.g., Christensen, 1966; Huber, 1981; Unruh, 1991; Wakabayashi and Sawyer, 2001). This assertion was challenged first by U/Th-He dating of erosion (House et al., 1998, 2001) and later by isotopic measurements inferred to reflect isotopic fractionation of precipitation associated with topography (Cassel et al., 2009, 2012; Mulch et al., 2006, 2008; Poage and Chamberlain, 2002). Although this interpretation remains controversial (Galewsky, 2009a, 2009b; Jones et al., 2004; Molnar, 2010), inferences that the Sierran crest lost an antibuoyant root between 10 and 3 Ma (Ducea and Saleeby, 1996, 1998; Farmer et al., 2002; Manley et al., 2000) suggested a "Sierran paradox" of an old range with a young means of support

(Wernicke et al., 1996). Quantifying the contributions of compositional and thermal variations of crust and mantle to the modern support of the range can help to resolve this controversy and highlight areas where a dynamic component (here defined as one that arises from the convective regime rather than directly from density variations) is necessary.

The 2005–2007 Sierra Nevada EarthScope Project (SNEP) deployment of FlexArray broadband seismometers across much of the Sierra Nevada has led to a much fuller three-dimensional characterization of the seismic structure of the range (Frassetto et al., 2011; Gilbert et al., 2012; Reeg, 2008). With such data we quantify the present-day distribution of density consistent with seismic and topographic constraints of the region. The simple assumptions that seismic wave speeds vary because of temperature variations in the mantle and because of a combination of compositional and temperature variations in the crust adequately recover topography. We thus do not find any need for dynamic topography in the region. Furthermore, the derived density variations can then be interpreted to limit the range of plausible means of supporting the topography and thus the tectonic history of the region.
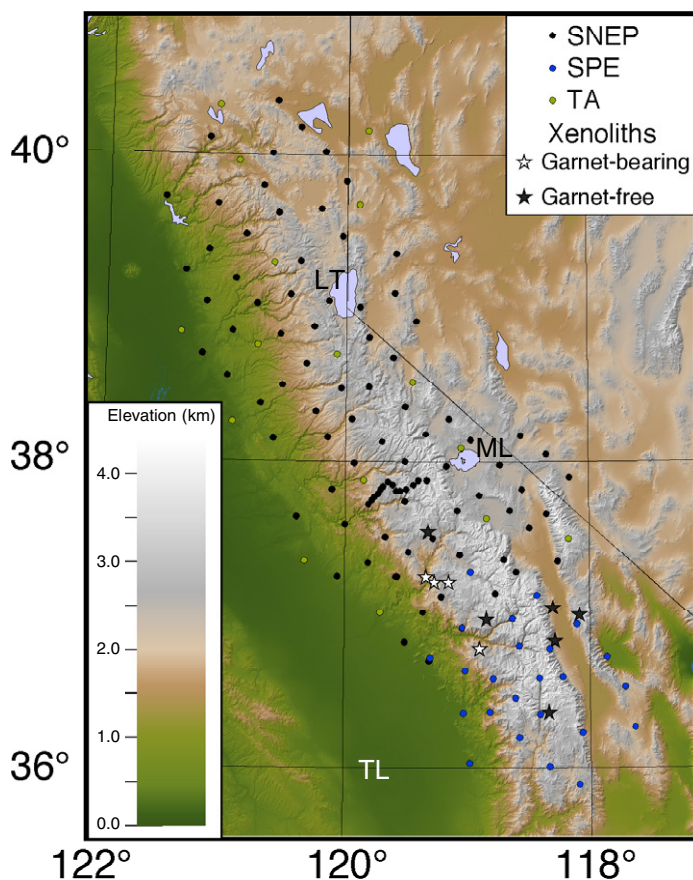
METHOD

It is useful to separate the contribution to topography (i.e., elevation above sea level) from the crust (H_c) from that from the mantle (H_m). We follow Lachenbruch and Morgan (1990), and define the following:

$$\varepsilon = H_c + H_m - H_0, \qquad (1)$$

where the crustal and mantle topography are

$$H_c = \int_{-\varepsilon}^{z_c} \frac{\rho_a - \rho(z)}{\rho_a} dz \qquad (2a)$$

Figure 1. The Sierra Nevada region topography (compare to Fig. 2A, flexurally smoothed topography). Also shown are key geographic features: Lake Tahoe (LT), Mono Lake (ML), and Tulare Lake (TL). Seismic stations used in the tomographic inversion (Jones et al., 2014) are from the Sierra Nevada Earthscope Project (SNEP), the Sierran Paradox Experiment (SPE), and the Earthscope Transportable Array (TA). Miocene and younger xenolith localities in the southern Sierra Nevada separated into garnet bearing (west) and garnet free (east).
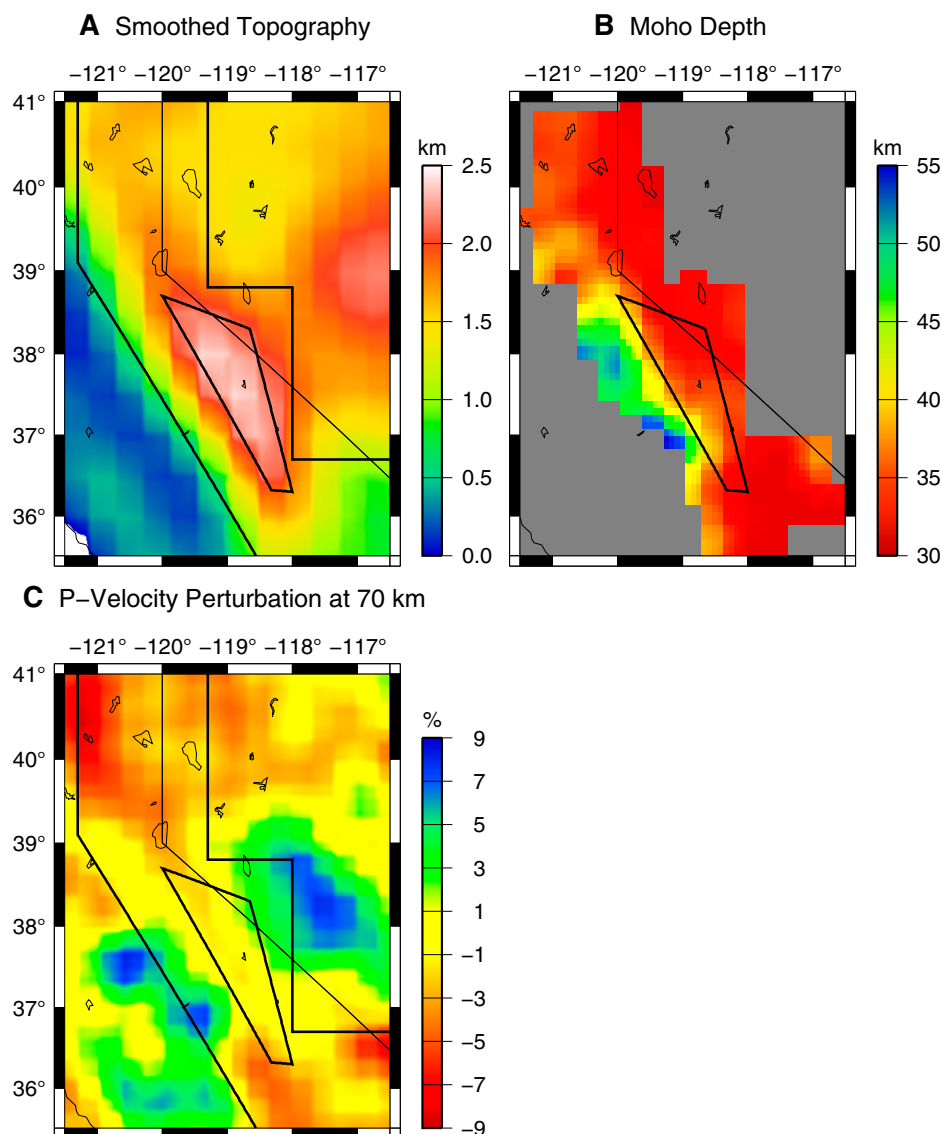
Seismic Velocity Model

Jones et al. (2014) present seismic velocity models derived from inversion of traveltime residuals subject to an array of starting models. Because teleseismic P-wave tomography has notoriously poor vertical resolution (especially in the crust), we choose a tomography model that was derived from an inversion where the top 55 km of the starting model was defined by ambient noise and earthquake surface wave tomography (Moschetti et al., 2010). The top of the starting model was held fixed for 14 of 21 iterations of the inversion, then allowed to vary as necessary to best fit teleseismic P-wave delay times. Because of the greater depth sensitivity of surface waves (at the cost of lateral resolution), this inversion scheme provides a more robust view of crustal velocity variations than would be available from teleseismic P-wave tomography alone. We have also completed our analysis with each of the other inversion schemes described by Jones et al. (2014) from a variety of starting models. Our results are generally robust with respect to seismic models, excepting the statistically significant difference arising in west-central Nevada, outside of the Sierra Nevada region with which we are primarily concerned.

Effect of Moho Variation on Velocity

Because we use different relationships between velocity and density (discussed in the following) in the crust and the mantle, we divide the tomography at the Moho depths determined in Frassetto et al. (2011). Nevertheless, the tomography of Jones et al. (2014) was calculated assuming a flat Moho. Thus, while we consider crustal thickness variations in estimated densities and crust- and/or mantle-derived topography, we must also adjust the teleseismic tomography for biases introduced by variable crustal thickness. This correction and its second-order effect on predicted topography are described in Appendix 1.

Mantle Density Estimation

We calculate the mantle-derived topography by assuming that density and wave speed variation is due to thermal heterogeneity. Isobaric heating will produce a decrease in both density and seismic velocity. Over a wide variety of lherzolite, harzburgite, and peridotite mineralogies the temperature derivatives of density are nearly equal, although the absolute densities vary considerably (Hacker and Abers, 2004). Therefore, we make no assumption of mantle mineralogy other than that it is laterally constant across the study area at any depth. Using a com-

$$H_\mathrm{m} = \int_{z_\mathrm{c}}^{z_\mathrm{a}} \frac{\rho_\mathrm{a} - \rho(z)}{\rho_\mathrm{a}} dz. \qquad (2b)$$

H_0 is a correction term of 2.4 km to achieve isostatic equilibrium with an asthenospheric column (via mid-ocean ridges). The depth of the Moho as defined by receiver functions is z_c (Frassetto et al., 2011). In this study, we examine to a depth, z_a, of 195 km based on the loss of correlation between seismic velocity and topography below this depth. The density of the asthenosphere is ρ_a and is assumed to be 3250 kg/m³. Because the motivation of this study is to explore the source of heterogeneity in the region, the exact choice of reference parameters (including asthenospheric density and crustal velocity) is of second-order importance. The value ε is the elevation above sea level with elastic flexural effects removed (Fig. 2A) by smoothing by convolution with a zero-order Bessel function (Watts, 2001; discussed in the following).

In order to calculate the topography generated by the crust and mantle, we convert the P-wave speeds from the seismic tomography (Reeg, 2008; Jones et al., 2014) into a density profile for each column, with a division at the Moho. Separating the support for smoothed topography into crustal and mantle components is necessary because we use different approaches in the crust and mantle to derive densities from seismic wave speeds. Seismic data from SNEP are used to constrain crustal thickness (using receiver functions; Frassetto et al., 2011) and wave speed variations in the crust and upper mantle (from P-wave tomography; Jones et al., 2014).

A Smoothed Topography

B Moho Depth

C P–Velocity Perturbation at 70 km

Figure 2. (A) Elevation in the Sierra Nevada region that has been smoothed by the Green's function response to point load topography, given a flexural parameter of 42 km (elastic thickness ~15 km). Note the >2 km discrepancy between southern Sierra Nevada and western foothills. For reference, the region with reliable receiver functions (see Fig. 2B) is outlined by a larger polygon. Range crest (mean elevation >~2 km) is outlined in smaller quadrilateral. (B) Receiver function–derived crustal thicknesses (from Frassetto et al., 2011). Note that the thickest crust is beneath the topographically lowest region. (C) Velocity perturbation of the 55–95 km layer (Jones et al., 2014). Note the high-velocity material beneath the foothills, neutral velocity beneath the southern Sierra Nevada, and low velocity in the southern Cascades and Basin and Range.

positionally independent conversion of velocity anomalies to density anomalies, we can then constrain the mantle contributions to isostasy for a purely thermally varying mantle, interpreting P-wave speed variations reported by Jones et al. (2014) as temperature variations and calculating the resulting density structure.

Laboratory data (Jackson and Faul, 2010) show a nonlinear dependence of shear modulus on temperature, particularly within 150–250 °C of the solidus. For this reason, we employ a decay in the density response to decreasing velocity for negative velocity perturbations, assuming that mean velocities in the upper mantle reflect temperatures of ~1050–1200 °C. This assumption is justified by estimates of minimum temperatures. At low temperatures velocity decreases <1% per 100 °C (Hacker and

Abers, 2004). Thus, a region with perturbation 5.5% (the maximum observed at 120 km) has a temperature at least 600 °C colder than background. This would correspond to a temperature (*T*) of <600 °C, which we take as a reasonable lower limit at this depth.

Between 0% and –3% velocity anomaly, our estimate of δρ/δVp decreases from 10 to 6 kg/m^3 per 1% velocity anomaly. This choice of parameters simulates the behavior of a variety of lherzolite, peridotite, and harzburgite mineralogies in the absence of anelasticity (i.e., at low temperature) (Hacker and Abers, 2004) and elastic response similar to that of millimeter-scale single crystal grains of olivine (Jackson and Faul, 2010). A schematic of the curvilinear relationship between velocity and density in the mantle is presented in Figure 3.

We also consider another end-member regression, a linear relationship between mantle velocity and density with no attempt to account for possible anelastic effects, but we find that our interpretations are relatively insensitive to the choice of regression (see discussion of results).

We note that P-wave speed variations caused by melt (–3.6% per 1% in situ melt fraction) (e.g., Hammond and Humphreys, 2000) produce disproportionately small changes in bulk density (between 0 and 4 kg/m^3 per 1% in situ melt fraction) that will cause the magnitude of variation in H_m to be too great. Because melt production and ponding depends on many parameters, we do not explicitly incorporate this effect in our wave speed–density relationship, but consider this effect later.

With this mantle topography (Fig. 4A) we examine the thermal and chemical variations in the crust.

Crustal Density Estimation

Seismic anomalies in the crust likely reflect variations in composition or temperature. We first convert P-wave speeds to density within the crust using regressions of density onto P-wave speed. We use velocities and densities reported by Christensen and Mooney (1995), correct the room-temperature densities reported for the temperature at which velocities are reported (using the coefficients of thermal expansion from the same compilation and using their average, ~15 °C/km geotherm), and regress density onto velocity for all nonvolcanic and polymineralic rocks and for dunite and pyroxenite. From 0 to 10 km, ρ = 827.5 + 316.6 × Vp. From 10 to 30 km, ρ = 643 + 337 × Vp; from 30 km to the Moho, ρ = 552.0 + 350.5 × Vp. Because the velocity structure reported by Jones et al. (2014) is a perturbation from mean wave speeds, we also choose a reference velocity structure of
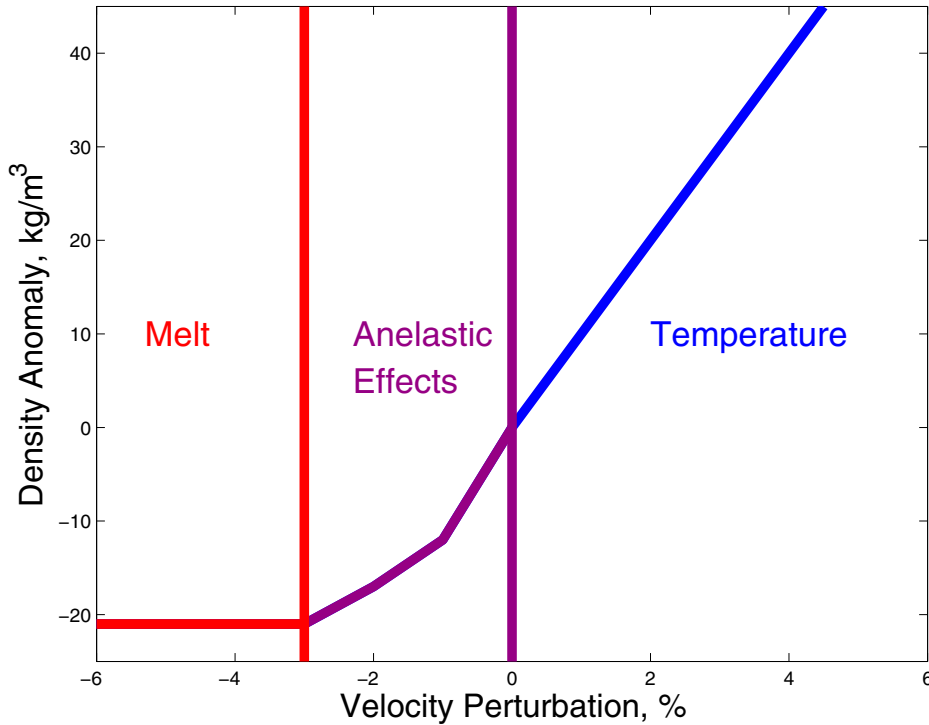
Figure 3. Mantle velocity-density relationship based on purely thermal effects. At low temperatures (positive velocity perturbations), the relationship is linear with a slope of 10 kg/m³ per 1% velocity change (~100 °C). Between 0% and –3% (~200 °C heating) velocity perturbation, anelastic effects begin to dominate, increasing the velocity change for a unit temperature increase while density is still a linear function of temperature. At velocities >–3% (>200 °C above background), we assume that material is above the solidus. Increased thermal input produces more melt, lowering velocity further, while melt has a very similar density to rock of the same temperature and thus bulk density remains constant (Hammond and Humphreys, 2000).

We employ the thermal-compositional basis in velocity-density space to generate a thermal structure that reproduces both velocities and topography.

For example, a region with 3% velocity perturbation might need a maximum 47 kg/m³ average density anomaly in the crust relative to the background structure to be in isostatic equilibrium within uncertainty. As discussed herein, a purely compositional source of heterogeneity would predict a 65 kg/m³ density anomaly. To decrease this density anomaly to 47 kg/m³, at least 50% of the velocity perturbation (1.5%, or 0.098 km/s for a 6.5 km/s background) is assigned to temperature. Following Equation 3, this crustal section is then at least 195 °C cooler on average than background.
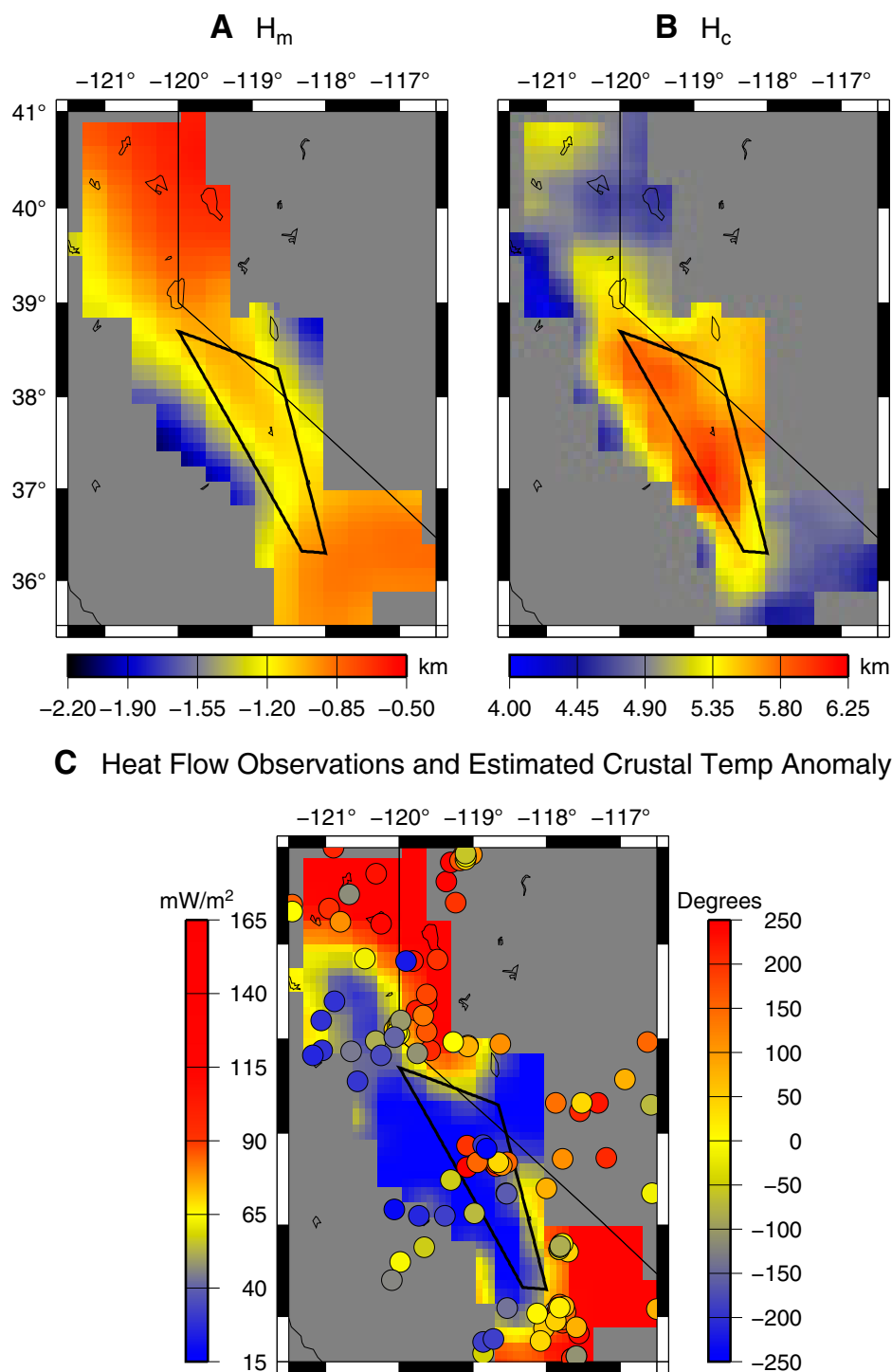
We limit the thermal perturbation to a geologically plausible range of ±250 °C. Miocene Moho paleotemperatures of ~350 °C (Molnar and Jones, 2004) are probably a lower bound on plausible Moho temperatures and are ~1000 °C below asthenospheric potential temperatures (1350 °C). Thus, the Miocene crustal column would have an average temperature anomaly of 500 °C below the hottest plausible crust if geotherms are approximately linear. Given these limits, we calculate crust-derived topography (Fig. 4B) that is a combination of thermal and chemical factors. This quantity represents an attempt to satisfy Equation 5 subject to the limits on allowable thermal variations in the crust discussed.

The result of these calculations compares well with thermal constraints from surface heat flow (Figs. 4C, 4D). The regions in which colder crustal geotherms are employed match almost exactly with areas of low reduced heat flow (Saltus and Lachenbruch, 1991) and low surface heat flow (Erkan and Blackwell, 2009), <25 mW/m² and 40 mW/m², respectively (Fig. 4C).

Vertical Stress Coupling

We recognize that loads in the sublithospheric mantle are only partially coupled to the overlying crust and surface. Deeper loads (from velocities at 120 km and 170 km depth nodes) are reduced in amplitude to account for viscous response in the upper mantle (50% and 25% coupling, respectively) (Parsons and Daly, 1983). This reduction is an approximation, as the degree of reduction in topographic expression is a function of wavelength and viscosity structure. We have chosen these factors to be approximately correct for loads with wavelengths of ~100 km in an isoviscous mantle. Between end-member cases of full coupling and complete decoupling of the lower 100 km of the model from the surface, the mean change (absolute value) in predicted elevation at any given node is 140 m. Our

5.8 km/s from the surface to 10 km, 6.5 km/s from 10 to 30 km depth, and 6.8 km/s from 30 km to the Moho based on a tomographic model determined using regional seismicity (Thurber et al., 2009).

The initial assumption of an isothermal crust maximizes crustal density variations. For example, a 3% increase in velocity from our reference at 20 km (Vp = 6.5 km/s, ρ = 2879 kg/m³) due to compositional variations predicts a ~65 kg/m³ higher density.

If, however, the velocity change, ΔVp, is due to a thermal perturbation, ΔT, then the density change is given by $\Delta\rho = \rho_0\alpha\Delta T$, and because

$$\Delta T = \Delta\mathrm{Vp}/(\partial\mathrm{Vp}/\partial T), \qquad (3)$$

then

$$\Delta\rho = \rho_0\alpha\Delta\mathrm{Vp}/(\partial\mathrm{Vp}/\partial T) \qquad (4)$$

with a known coefficient of thermal expansion, α. If the 3% velocity increase (0.195 km/s) discussed here was because this crust was colder

than our reference, from Equation 4 the density would only increase ~28 kg/m³, assuming a coefficient of thermal expansion of 2.5 × 10⁻⁵ °C⁻¹ and a ∂Vp/∂T of –0.5 m/s °C⁻¹ (Christensen and Mooney, 1995). Thus, from Equation 3 this region is 195 m/s per 0.5 m/s °C⁻¹, or 390 °C colder than reference.

Because of the linear independence of velocity-density scaling vectors, one for thermal effects and the other for compositional changes, one can employ them as a basis and thus match any arbitrary velocity-density data point. Given an estimate of mantle-derived topography, we thus calculate the crustal buoyant height necessary to match topography from Equation 1:

$$H_c = \varepsilon + H_0 - H_m. \qquad (5)$$

From this value we make use of knowledge of crustal thickness to calculate the mean crustal density necessary (from Equations 2a, 2b):

$$\overline{\rho}_c = \rho_a\left(1 - \frac{H_c}{z_c}\right). \qquad (6)$$

Figure 4. (A) Mantle topography calculated for the Sierra Nevada region for the purely thermal variation described in the text. Of particular note is the heterogeneity between the foothills (~–1.75 km) and the Sierra Nevada (~–0.75). (B) Crustal topography calculated for the Sierra Nevada region for the combined thermal-compositional variation described in the text. Of particular note is the heterogeneity between the foothills (H_c ~ 5 km) and the Sierra Nevada (H_c ~ 6 km). Also notable is the low buoyancy calculated for the southern Cascades and Basin and Range. (C) Background: Estimated mean thermal perturbation (half of Moho temperature variation), derived using the thermal-compositional basis described in the text. Scale on right. Overlay: Observed heat flow points (e.g., Erkan and Blackwell, 2009) for reference. Scale at left.

approximation cannot produce errors of greater mean absolute value than 100 m, the difference from the fully coupled end member.

Flexural Considerations

By smoothing the elevation field, we remove the effect of short-wavelength topographic variations generated by erosion and/or deposition, fault displacement, and volcanism (i.e., removing the surface loads of Lowry et al., 2000). The elastic filter is based on an estimate of flexural rigidity (3.5×10^{22}, elastic thickness 18 km) from basin geometry of the San Joaquin Valley, adjacent to the range (in accord with Saleeby and Foster, 2004). Although elastic thickness may differ across the region, varying the elastic thickness from 5 to 30 km changes our predicted topography by <250 m and not in a manner affecting the overall pattern of our results. Because flexural loads adjoining our study area will influence topography, we examined these edge effects by extending our study outward 100 km into the region with tomographic coverage but no reliable receiver functions (and assuming a crustal thickness similar to the nearest receiver function). These effects are <200 m for models with 15 km elastic thickness and only affect the margins of our model.

The crustal and mantle topography are smoothed by the same flexural filter.

ERROR ANALYSIS

Random Error

Uncertainties in seismologically based estimates of topography are calculated from the errors of the parameters used. The most important parameters in our error analysis are the velocity-density relations (Christensen and Mooney, 1995; Hacker and Abers, 2004; Jackson and Faul, 2010), wave speed perturbations, crustal thickness variations, and background asthenospheric density. Uncertainties (2σ) are estimated as 60 kg/m³ for the velocity to density conversion (Christensen and Mooney, 1995), 0.25% for velocity perturbation in the mantle, 3 kg/m³ per 1% Vp perturbation, and 50 kg/m³ for asthenospheric density. Crustal thickness uncertainties were given in Frassetto et al. (2011) and range between 1 and 5 km. These values yield typical 2σ uncertainties of the resulting synthetic topography of ~600 m (Fig. 5A).

Systematic Error

Systematic biases in our analysis may also be present to the degree that the seismic data (tomography and receiver functions) are sys-

A Uncertainty   **B** H_r

C H_r +/− Uncertainty, Anelastic Scaling   **D** H_r +/− Uncertainty, Linear Scaling
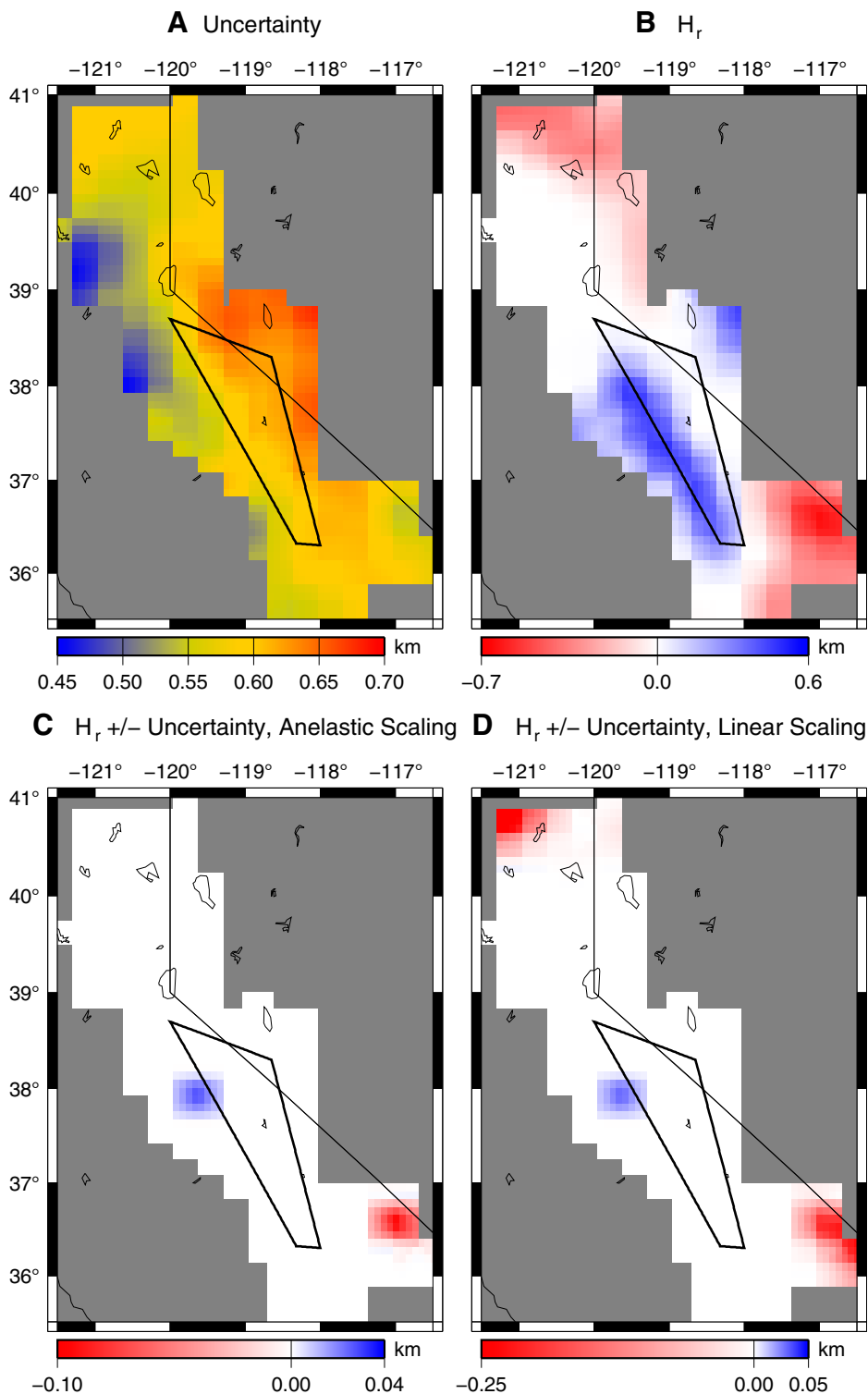
Figure 5. (A) Uncertainties (2σ) in topographic prediction. Typical values are ~600 m. (B) Residual topography (H_r; observed elevation minus predicted elevation). (C) Residual topography with 2σ uncertainties removed. Nodes with residual magnitude within uncertainty are displayed as zero. Note change in scale from B. (D) Same as C, but with densities linearly proportional to velocity (10 kg/m³ per 1% velocity perturbation) even at high temperatures.

tematically biased. While traveltime delay along a ray path is a robust observation in traveltime tomography, the depth extent of velocity anomalies is less certain. We therefore consider the effects of the limited vertical resolution of teleseismic tomography, in particular the placement of anomalies from the mantle into the crust or vice versa. We have therefore conducted the same analysis under the physically unreasonable end-member cases that all traveltime anomalies produced in the top 95 km are due to wave speed variations solely in the crust or solely in the mantle. Because the velocity to density scaling relationships are different in the two domains but of the same polarity, the effect is one of magnification. Heterogeneities in predicted elevation (and thus residual topography) are maximized if the mantle is homogeneous and the crust is responsible for all traveltime delays. Because forcing all wave speed variations into the crust generates crustal velocity heterogeneity of several tens of percent, values well beyond plausible, this calculation bounds our estimated topography's sensitivity to systematic biases in the tomography. The mean magnitude of change is <100 m, and ~95% of the elevation predictions are affected by <400 m.

A similar end-member investigation explores the robustness of our observations in the face of receiver function errors. In our analysis, we have treated the crust-mantle boundary as laterally variable. Nevertheless, identification of the Moho in many areas, especially those with a Moho significantly different from ~35–40 km depth, is challenging (Frassetto et al., 2011). Therefore, we explored similar topography calculations with a constant crustal thickness. To a great degree, the results of calculations with this architecture are consistent with those honoring receiver functions, as the practical effect of this change is to change the domain (crust or mantle) in which velocity anomalies are located, and consequently predicted elevations differ by as much as ~100 m.

Furthermore, anelastic effects are not considered in the crust. The signature of low crustal velocities (thus high H_c) and high estimated crustal temperatures might be indicative of supersolidus temperatures. If melt is present in the crust, density estimates will be too low (as described herein), and positive gravity residuals will be produced.

REAULTS

We have generated a lithospheric density model derived from seismic wave speeds and a crustal thermal regime calculated to most closely match observed topography (summarized in Figs. 4A, 4B). Where these combined crustal and mantle buoyancy variations repro-

duce observed topography, we suggest that these variations are responsible for supporting the topography in the region. Elsewhere, other effects could be present, which could reflect the presence of (especially crustal) melt, dynamic topography (arising from convection-derived stress), compositional variations in the mantle, or compositional variations in the crust beyond those represented by the regressions of data from Christensen and Mooney (1995). To identify these areas more clearly, we calculate the residual topography H_r (Fig. 5B), which represents the smoothed topography (Fig. 2A) minus the calculated topography.

$$H_r \equiv \varepsilon + H_0 - H_c - H_m. \qquad (7)$$

As seen in Figure 5B, elevations in much of the study area are nearly matched by a combination of compositional and (geologically reasonable but not directly observed) thermal variations in the crust and thermal variations in the mantle. Furthermore, nearly all of the misfit is within the uncertainty of topography estimates (Fig. 5C).

To explore possible errors from our scaling of mantle velocity into density, we also calculated results assuming a linear velocity-density relationship (i.e., one lacking correction for possible anelastic effects). The results are nearly identical (Fig. 5D), but with an additional –400 m of residual topography in the southern Cascades and southwesternmost Great Basin, near Death Valley. This residual is consistent with small amounts of partial melt or with anelastic effects, similar to the interpretations made here.

GRAVITY

A logical test of our three-dimensional density model is a comparison with the observed Bouguer gravity anomaly, although we note that the limited ability to resolve the vertical position of density anomalies within the crust will lead to large uncertainties, even at the >100 km wavelengths of greatest interest here, and the limited width of the study area means that significant gravity anomalies could be generated from outside the model. Plausible ranges in density structures fitting the gravity field alone were illustrated in Kennelly and Chase (1989) and Jones et al. (1994). We have calculated the Bouguer gravity field predicted by our seismically derived density model (Fig. 6B), which largely recovers the observed Bouguer gravity variations (Fig. 6A). The most striking feature of a Bouguer gravity map of the region is the ~300 mGal decrease from the foothills to the range crest. Our model recovers >200 mGal decrease into the range. Our model also recovers Bouguer gravity along range strike both north-northwest and south-southeast
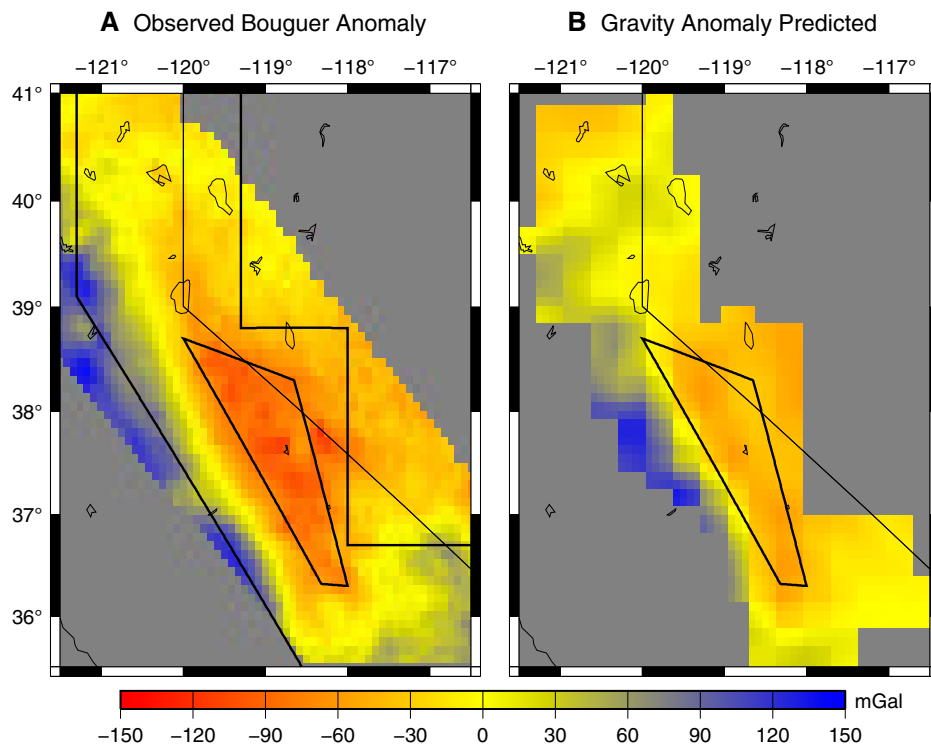
Figure 6. (A) Bouguer gravity variations (i.e., regional mean removed) from the National Oceanic and Atmospheric Administration National Geophysical Data Center 1999 database (Dater et al., 1999). (B) Map of demeaned Bouguer gravity field derived from density model. Areas outside of study are assumed to have neutral density.

of the range crest. Remaining differences reflect a combination of masses outside the model bounds and the uncertainty in the vertical placement of density anomalies in the crust.

We note here that our gravity model seems to preclude the presence of variations in dynamic topography. To illustrate, consider a region at sea level with isopycnic mantle lithosphere (i.e., H_m = 0) and 40-km-thick crust of uniform density. If in isostatic equilibrium (i.e., H_c = 2.4 km), the crust must be 3008 kg/m³. If a ~1 km of dynamic topography (basal normal force of ~30 MPa) is being generated by asthenospheric convection (i.e., H_c = 1.4 km), then crustal density is 3088 kg/m³. The difference in the gravity signal from these two crustal columns is ~135 mGal in the infinite slab limit and 118 mGal if active over a 300 km wavelength. Thus, given the absence of large-magnitude gravity residuals, we argue that the density structure that we estimate, and not dynamic topography, is responsible for the modern topographic relief of the Sierra Nevada.

DISCUSSION

In our model, the mean crustal density is estimated to be between 2900 and 3000 kg/m³ beneath the foothills and ~2750–2800

kg/m³ beneath the range crest (Fig. 7B). The ~50–55-km-thick foothills crust provides ~5 km of topography while the thinner (40–45 km thick) but lighter crust under the range crest provides ~6 km of topography (Fig. 4B).

The remaining ~1 km topographic difference between the two areas is generated within the upper mantle (Fig. 7D). There is a 10% velocity increase (Jones et al., 2014) over a lateral distance of ~150 km from beneath the range crest southwestward into the foothills (Fig. 2C). With the anelastic scaling described here (following Hacker and Abers, 2004; Jackson and Faul, 2010), this velocity anomaly (if due as assumed to thermal variation alone) represents a density contrast of 84 kg/m³. Thus 1.0 km of relief is caused by this upper mantle anomaly, a magnitude comparable to the relief caused by crustal buoyancy variations.

As an alternative to decomposing the topography field spatially, into crustal and mantle components (Figs. 4A, 4B), one can separate topography mechanistically into thermal, compositional, and dynamic components. We present such decomposition in Figure 7, where all values are demeaned. Because we succeed in explaining topography (within uncertainty) in nearly all of the study area and closely recov-
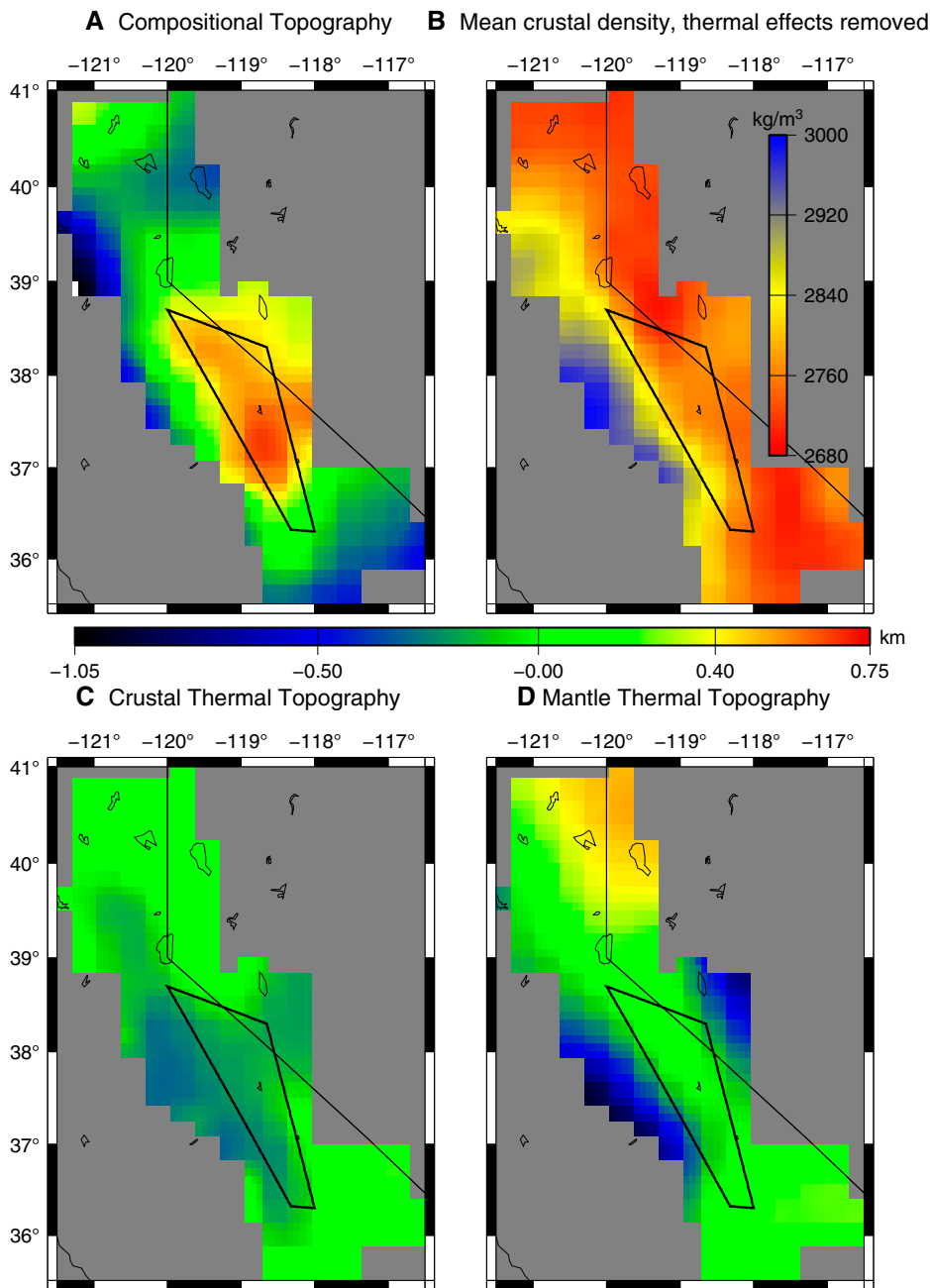
Figure 7. (A) Compositional topography: crustal topography H_c (see Fig. 4B) minus thermal contribution and with the mean value removed. Note the contrast between the southern Sierra range crest and regions north-northwest and south-southeast. (B) Mean crustal density with estimated thermal effect removed. Note the gradient from east-northeast to west-southwest (Basin and Range to Sierra Nevada to foothills). The greater density of the foothills crust is due principally to chemistry, not temperature. (C) Crustal thermal topography. Note the small magnitude of variation compared to mantle thermal (D) and crustal compositional (A) contributions. Peak (Death Valley region) to trough (western foothills) amplitude is ~500 m. (D) Mantle thermal topography: same as mantle contribution, H_m (Fig. 4A), but with the mean removed. Of particular note is the heterogeneity between the foothills (~–1 km) and the Sierra Nevada (~0 km).

ering gravity, with purely thermal variations in the mantle, we limit the need for chemical variations in the mantle or a spatially varying dynamic component to topography to less than our uncertainty of ~600 m. Thus, compositional topography (Fig. 7A) is simply crustal topography (Fig. 4B) with the crustal thermal topography (Fig. 7C) removed. Comparing the foothills to the range crest, we find little (~100 m) difference in crustal thermal topography. Conversely, the mantle underlying the foothills provides ~1 km less thermal support than under the range crest (Fig. 7D). The remaining 1 km of discrepancy is due to crustal composition and thickness (Fig. 7A).

These findings are consistent with the conceptual model proposed previously (e.g., Ducea and Saleeby, 1996; Jones et al., 2004; Le Pourhiet et al., 2006; Molnar and Jones, 2004; Saleeby et al., 2012; Zandt et al., 2004), that negatively buoyant material has been removed from the mantle beneath the southern Sierra Nevada and is now foundering to the west of the range. If the mantle beneath the range crest had resembled that of the foothills until the Miocene, elevations would have been ~1 km lower. If either a thicker thermal boundary layer or compositionally anti-buoyant mantle lithosphere had existed beneath the batholith, more uplift is admissible.

The ~35-km-thick crust in the Sierra Nevada has relatively low velocities that are mainly due to lithology, rather than to high temperatures. The crust is thinner by 5–10 km but slower by ~0.25 km/s beneath the Basin and Range and Cascades than beneath the Sierra Nevada. We propose that the lower wave speeds in the Death Valley region are due not to composition but to higher crustal temperatures and perhaps small average amounts of partial melt. The crust in the Death Valley region may be chemically denser (and thinner) than beneath the Sierra Nevada, and thus supports 1 km less topography than crust under the Sierra.

CONCLUSIONS

Beginning from seismic velocities, we have created a density structure in the Sierra Nevada region that reproduces modern topography and is nearly concordant with the observed gravity field. The model assumes thermal and chemical heterogeneity in the crust and temperature variations in the mantle, but we find no need for topography derived from mantle chemistry or asthenospheric convection (i.e., dynamic topography) in order to recover observed elevations. Uppermost mantle densities account for ~1 km of relief between the Sierran crest and foothills. If such material was present beneath the range in the Miocene, we estimate ~1 km

of surface uplift upon its removal and regional isostatic equilibration. Our work is consistent with the hypothesis that cold upper mantle has been removed from the southern Sierra Nevada but not the western foothills. Chemically buoyant crust of moderate thickness beneath the high southern Sierra Nevada supports >1 km of topography relative to the thinner, warmer, chemically denser crust of the Basin and Range and southern Cascades.

ACKNOWLEDGMENTS

APPENDIX: EFFECT OF MOHO VARIATION OF WAVE SPEED ESTIMATES

We here detail the means of reconciling the variations in Moho depth with the P-wave structure derived assuming a flat Moho. Consider two locations with identical teleseismic P-wave speed anomalies but different Moho depths. To honor the teleseismic delay times, the integrated traveltime along teleseismic ray paths must be the same as that calculated with no Moho variation. Where the Moho is deeper, crustal and/or uppermost mantle wave speed anomalies must be higher than directly computed from the P-wave tomography, because rays must traverse a thicker section of crustal material that is initially assumed to have a lower Vp than the mantle. For example, a 10-km-thick section of lower crust (Vp = 6.8 km/s) is expected to result in a 0.23 s delay relative to 10 km of asthenosphere (Vp = 8.04 km/s).

To derive appropriate wave speed models, we compute an expected delay time relative to the background model of a 37-km-thick crust with three crustal layers overlying an uppermost mantle of velocity 8.04 km/s from varying Moho depths separating a homogeneous crust from a homogeneous mantle. This effect of variations in crustal thickness, Δt_{Moho}, can be expressed as

$$\Delta t_{Moho} = \int_{z_c}^{\varepsilon} \frac{dz}{\overline{v}_c(z)} + \int_{95\,km}^{z_c} \frac{dz}{\overline{v}_m(z)} - t_{ref}, \quad (A1)$$

where velocities are as described in the text, z_c is the crustal thickness at a given point, and where

$$t_{ref} = \int_{z_c}^{\varepsilon} \frac{dz}{\overline{v}_c(z)} + \int_{95\,km}^{z_c} \frac{dz}{\overline{v}_m(z)} \quad (A2)$$

is the traveltime from the surface to 95 km through a reference model of a 37-km-thick crust with the previously described crustal velocities underlain by 8.04 km/s mantle. Thus, a region with thick crust is predicted to have a positive delay time; incoming energy traverses a longer path of lower wave speed crustal material. This artifact of crustal structure can be corrected by adjusting the mean velocity perturbations from the P-wave tomography. The mean wave speed perturbation (dVp) to be removed is, when averaged over the same 95 km depth interval,

$$d\text{Vp}_{Moho} = -\left(\Delta t_{Moho}/t_{ref}\right) \times 100. \quad (A3)$$

A region of thick crust would be expected to show positive time delay; if reported to have slightly negative velocity perturbation, the compositional and thermal source of wave speed changes may be near zero. Removing this velocity perturbation reported from that by Jones et al. (2014) leaves only the velocity perturbations that reflect lateral variations in composition or temperature:

$$d\text{Vp}'(z) = d\text{Vp}(z) - d\text{Vp}_{Moho}. \quad (A4)$$

We assign this deviation uniformly through the seismic model from the surface to 95 km. We use such a broad area for three reasons. First, this avoids generating large, probably unrealistic velocity anomalies adjacent to the Moho. Second, this approach is consistent with inversions of synthetic data sets (Reeg, 2008; Jones et al., 2014) that show that vertically compact velocity anomalies at these depths will tend to be smeared vertically over several adjacent layers in the tomographic model. Third, because the pertinent quantity in P-wave tomography is integrated delay time along the raypath and the pertinent quantity is prediction of topography is the integrated density through the lithospheric column, the predicted topography is virtually unaffected by this smearing and so is a robust result of the tomographic inversion. Loss of vertical resolution is accompanied by a decreased magnitude of the anomaly such that the predicted topography integral is within 2% in the case of a checkerboard test (without any discrepancy between crust and mantle); the low pass filter of lithospheric flexure further smooths the surface response.

Modulating absolute Vp would have a small effect on receiver function interpretations conducted without such changes. The greatest Moho depth (55 km) results in a dVp$_{Moho}$ of 3.0%. If the mean crustal Vp is 6.5 and Vp/Vs is 1.8, then the difference between Ps and direct P travel time ts-tp=6.77s. Honoring this delay time and perturbing Vp and Vs by 3% (to 6.695 and 3.72 km/s, respectively) will lead to a Moho depth estimate of 56.65 km. In turn, a 1.65-km-thick section of lower crust with dVp = 3% provides of 43.5 m of topography while a 1.65-km-thick section of upper mantle with dVp = 3% supports –15.5 m of elevation. The most extreme changes necessary would therefore be 1.65 km crustal thickness and 59 m in predicted elevation.

REFERENCES CITED

Cassel, E.J., Graham, S.A., and Chamberlain, C.P., 2009, Cenozoic tectonic and topographic evolution of the northern Sierra Nevada, California, through stable isotope paleoaltimetry in volcanic glass: Geology, v. 37, p. 547–550, doi:10.1130/G25572A.1.

Cassel, E.J., Graham, S.A., Chamberlain, C.P., and Henry, C.D., 2012, Early Cenozoic topography, morphology, and tectonics of the northern Sierra Nevada and western Basin and Range: Geosphere, v. 8, p. 229–249, doi: 10.1130/GES00671.1.

Christensen, M.N., 1966, Late Cenozoic crustal movements in the Sierra Nevada of California: Geological Society of America Bulletin, v. 77, p. 163–182, doi:10.1130/0016-7606(1966)77[163:LCCMIT]2.0.CO;2.

Christensen, N.I., and Mooney, W.D., 1995, Seismic velocity structure and composition of the continental crust: A global view: Journal of Geophysical Research, v. 100, no. B7, p. 9761–9788, doi:10.1029/95JB00259.

Dater, D., Metzger, D., and Hittelman. A., compilers, 1999, Land and Marine Gravity CD-ROMs: Boulder, Colorado, U.S. Department of Commerce, National Oceanic and Atmospheric Administration, National Geophysical Data Center, 2 CD-ROMs.

Ducea, M.N., and Saleeby, J.B., 1996, Buoyancy sources for a large, unrooted mountain range, the Sierra Nevada, California: Evidence from xenolith thermobarometry: Journal of Geophysical Research, v. 101, no. B4, p. 8229–8244, doi:10.1029/95JB03452.

Ducea, M.N., and Saleeby, J.B., 1998, A case for delamination of the deep batholithic crust beneath the Sierra Nevada, California: International Geology Review, v. 40, p. 78–93, doi:10.1080/00206819809465199.

Erkan, K., and Blackwell, D., 2009, Transient thermal regimes in the Sierra Nevada and Baja California extinct outer arcs following the cessation of Farallon subduction: Journal of Geophysical Research, v. 114, B02107, doi:10.1029/2007JB005498.

Farmer, G.L., Glazner, A.F., and Manley, C.R., 2002, Did lithospheric delamination trigger late Cenozoic potassic volcanism in the southern Sierra Nevada, California?: Geological Society of America Bulletin, v. 114, p. 754–768, doi:10.1130/0016-7606(2002)114<0754: DLDTLC>2.0.CO;2.

Fliedner, M.M., Klemperer, S.L., and Christensen, N.I., 2000, Three-dimensional seismic model of the Sierra Nevada arc, California, and its implications for crustal and upper mantle composition: Journal of Geophysical Research, v. 105, no. B5, p. 10899–10921, doi:10.1029/2000JB900029.

Frassetto, A., Zandt, G., Gilbert, H., Owens, T.J., and Jones, C., 2011, Structure of the Sierra Nevada from receiver functions and implications for lithospheric foundering: Geosphere, v. 7, p. 898–921, doi:10.1130/GES00570.1.

Galewsky, J., 2009a, Orographic precipitation isotopic ratios in stratified atmospheric flows: Implications for paleoelevation studies: Geology, v. 37, p. 791–794, doi: 10.1130/G30008A.1.

Galewsky, J., 2009b, Rain shadow development during the growth of mountain ranges: An atmospheric dynamics perspective: Journal of Geophysical Research, v. 114, no. F1, doi:10.1029/2008JF001085.

Gilbert, H., Yang, Y., Forsyth, D.W., Jones, C.H., Owens, T.J., Zandt, G., and Stachnik, J.C., 2012, Imaging lithospheric foundering in the structure of the Sierra Nevada: Geosphere, v. 8, p. 1310–1330, doi:10.1130/GES00790.1.

Hacker, B.R., and Abers, G.A., 2004, Subduction factory 3: An Excel worksheet and macro for calculating the densities, seismic wave speeds, and H2O contents of minerals and rocks at pressure and temperature: Geochemistry Geophysics Geosystems, v. 5, doi:10.1029/2003GC000614.

Hammond, W.C., and Humphreys, E., 2000, Upper mantle seismic velocity: Effects of realistic partial melt geometries: Journal of Geophysical Research, v. 105, no. B5, p. 10975–10986, doi:10.1029/2000JB900041.

Holbrook, W.S., Mooney, W.D., and Christensen, N.I., 1992, The seismic velocity structure of the deep continental crust, *in* Fountain, D.M., et al., eds., Continental lower crust: Developments in Geotectonics 23: Amsterdam, Elsevier, p. 1–43.

House, M.A., Wernicke, B.P., and Farley, K.A., 1998, Dating topography of the Sierra Nevada, California, using apatite (U-Th)/He ages: Nature, v. 396, 6706, p. 66–69, doi:10.1038/23926.

House, M.A., Wernicke, B.P., and Farley, K.A., 2001, Paleogeomorphology of the Sierra Nevada, California, from (U-Th)/He ages in apatite: American Journal of Science, v. 301, p. 77–102, doi:10.2475/ajs.301.2.77.

Huber, N.K., 1981, Amount and timing of late Cenozoic uplift and tilt of the central Sierra Nevada, California— Evidence from the upper San Joaquin River basin: U.S. Geological Survey Professional Paper 1197, 28 p.

Jackson, I., and Faul, U.H., 2010, Grainsize-sensitive viscoelastic relaxation in olivine: Towards a robust laboratory-based model for seismological application: Physics of the Earth and Planetary Interiors, v. 183, p. 151–163, doi:10.1016/j.pepi.2010.09.005.

Jones, C.H., Kanamori, H., and Roecker, S.W., 1994, Missing roots and mantle "drips": Regional Pn and teleseismic arrival times in the southern Sierra Nevada and vicinity, California: Journal of Geophysical Research, v. 99, p. 4567–4601, doi:10.1029/93JB01232.

Jones, C.H., Farmer, G.L., and Unruh, J.R., 2004, Tectonics of Pliocene removal of lithosphere of the Sierra Nevada, California: Geological Society of America Bulletin, v. 116, p. 1408–1422, doi:10.1130/B25397.1.

Jones, C.H., Reeg, H., Zandt, G., Gilbert, H., and Owens, T.J., 2014, P-wave tomography of potential convective down-wellings and their source regions, Sierra Nevada, California: Geosphere, doi:10.1130/GES00961.1 (in press).

Kennelly, P.J., and Chase, C.G., 1989, Flexure and isostatic residual gravity of the Sierra Nevada: Journal of Geophysical Research, v. 94, no. B2, p. 1759–1764, doi:10.1029/JB094iB02p01759.

Lachenbruch, A.H., and Morgan, P., 1990, Continental extension, magmatism and elevation; formal relations and rules of thumb: Tectonophysics, v. 174, p. 39–62, doi:10.1016/0040-1951(90)90383-J.

LeConte, J., 1886, A post-Tertiary elevation of the Sierra Nevada shown by the river beds: American Journal of Science, v. 32, 189, p. 167–181, doi:10.2475/ajs.s3-32.189.167.

Le Pourhiet, L., Gurnis, M., and Saleeby, J., 2006, Mantle instability beneath the Sierra Nevada mountains in California and Death Valley extension: Earth and Planetary Science Letters, v. 251, p. 104–119, doi:10.1016/j.epsl.2006.08.028.

Lowry, A.R., Ribe, N.M., and Smith, R.B., 2000, Dynamic elevation of the Cordillera, western United States: Journal of Geophysical Research, v. 105, no. B10, p. 23371–23390, doi:10.1029/2000JB900182.

Manley, C.R., Glazner, A.F., and Farmer, G.L., 2000, Timing of volcanism in the Sierra Nevada of California: Evidence for Pliocene delamination of the batholithic root?: Geology, v. 28, p. 811–814, doi:10.1130/0091-7613(2000)28<811:TOVITS>2.0.CO;2.

Molnar, P., 2010, Deuterium and oxygen isotopes, paleo-elevations of the Sierra Nevada, and Cenozoic climate: Geological Society of America Bulletin, v. 122, p. 1106–1115, doi:10.1130/B30001.1.

Molnar, P.H., and Jones, C.H., 2004, A test of laboratory based rheological parameters of olivine from an analysis of late Cenozoic convective removal of mantle lithosphere beneath the Sierra Nevada, California, USA: Geophysical Journal International, v. 156, p. 555–564, doi:10.1111/j.1365-246X.2004.02138.x.

Moschetti, M.P., Ritzwoller, M.H., Lin, F.C., and Yang, Y., 2010, Crustal shear wave velocity structure of the western United States inferred from ambient seismic noise and earthquake data: Journal of Geophysical Research, v. 115, no. B10, doi:10.1029/2010JB007448.

Mulch, A., Graham, S.A., and Chamberlain, C.P., 2006, Hydrogen isotopes in Eocene river gravels and paleo-elevation of the Sierra Nevada: Science, v. 313, p. 87–89, doi:10.1126/science.1125986.

Mulch, A., Sarna-Wojcicki, A.M., Perkins, M.E., and Chamberlain, C.P., 2008, A Miocene to Pleistocene climate and elevation record of the Sierra Nevada (California): National Academy of Sciences Proceedings, v. 105, p. 6819–6824, doi:10.1073/pnas.0708811105.

Parsons, B., and Daly, S., 1983, The relationship between surface topography, gravity anomalies, and temperature structure of convection: Journal of Geophysical Research, v. 88, no. B02, p. 1129–1144, doi:10.1029/JB088iB02p01129.

Poage, M.A., and Chamberlain, C.P., 2002, Stable isotopic evidence for a pre-Middle Miocene rain shadow in the western Basin and Range: Implications for the paleo-topography of the Sierra Nevada: Tectonics, v. 21, no. 4, p. 16-1–16-10, doi:10.1029/2001TC001303.

Reeg, H., 2008, Seismic structure of the crust and upper mantle of the Sierra Nevada, California [M.S. thesis]: Boulder, University of Colorado, 139 p.

Ruppert, S., Fliedner, M.M., and Zandt, G., 1998, Thin crust and active upper mantle beneath southern Sierra Nevada: Tectonophysics, v. 286, p. 237–252.

Saleeby, J., and Foster, Z., 2004, Topographic response to mantle lithosphere removal in the southern Sierra Nevada region, California: Geology, v. 32, p. 245–248, doi:10.1130/G19958.1.

Saleeby, J., Le Pourhiet, L., Saleeby, Z., and Gurnis, M., 2012, Epeirogenic transients related to mantle litho-sphere removal in the southern Sierra Nevada region, California, part I: Implications of thermomechanical modeling: Geosphere, v. 8, p. 1286–1309, doi:10.1130/GES00746.1.

Saltus, R.W., and Lachenbruch, A.H., 1991, Thermal evolution of the Sierra Nevada; Tectonic implications of new heat flow data: Tectonics, v. 10, p. 325–344, doi:10.1029/90TC02681.

Simpson, R.W., Jachens, R.C., Saltus, R.W., and Blakely, R.J., 1986, Isostatic residual gravity, topographic, and first-vertical-derivative gravity maps of the conterminous United States: U.S. Geological Survey Geophysical Investigations Map GP-975, 4 sheets.

Thurber, C., Zhnag, H., Brocher, T., and Langenheim, V., 2009, Regional three-dimensional seismic velocity model of the crust and uppermost mantle of northern California: Journal of Geophysical Research, v. 114, no. B1, doi:10.1029/2008JB005766.

Unruh, J.R., 1991, The uplift of the Sierra Nevada and implications for late Cenozoic epeirogeny in the western Cordillera: Geological Society of America Bulletin, v. 103, p. 1395–1404, doi:10.1130/0016-7606(1991)103<1395:TUOTSN>2.3.CO;2.

Wakabayashi, J., and Sawyer, T.L., 2001, Stream incision, tectonics, uplift and evolution of topography of the Sierra Nevada, California: Journal of Geology, v. 109, p. 539–562, doi:10.1086/321962.

Watts, A.B., 2001, Isostasy and flexure of the lithosphere: Cambridge, Cambridge University Press, 458 p.

Wernicke, B., and 18 others, 1996, Origin of high mountains in the continents: The southern Sierra Nevada: Science, v. 271, p. 190–193, doi:10.1126/science.271.5246.190.

Zandt, G., Gilbert, H., Owens, T.J., Ducea, M., Saleeby, J., and Jones, C.H., 2004, Active foundering of a continental arc root beneath the southern Sierra Nevada in California: Nature, v. 431, 7004, p. 41–46, doi:10.1038/nature02847.